AMERICAN
METEOROLOGICAL
SOCIETY

Journal of Climate

EARLY ONLINE RELEASE

This is a preliminary PDF of the author-produced manuscript that has been peer-reviewed and accepted for publication. Since it is being posted so soon after acceptance, it has not yet been copyedited, formatted, or processed by AMS Publications. This preliminary version of the manuscript may be downloaded, distributed, and cited, but please be aware that there will be visual differences and possibly some content differences between this version and the final published version.

The DOI for this manuscript is doi: 10.1175/2010JCLI3341.1

The final published version of this manuscript will replace the preliminary version at the above DOI once it is available.

Regional Patterns of Sea Level Change Related to Interannual Variability and Multi-decadal Trends in the Atlantic Meridional Overturning Circulation

K. Lorbacher[1], *J. Dengg*[1], *C. W. Böning*[1] *and A. Biastoch*[1]

[1]*IFM-GEOMAR, Leibniz-Institut für Meereswissenschaften, Düsternbrooker Weg 20, 24105 Kiel, Germany.*

submitted to *Journal of Climate*

- REVISION -

2009-12-30

corresponding author: K. Lorbacher, klorbacher@ifm-geomar.de, ++49-431-6004159

Abstract

Some studies of ocean climate model experiments suggest that regional changes in dynamic sea level could provide a valuable indicator of trends in the strength of the Atlantic meridional overturning circulation (MOC). Here, we use a sequence of global ocean-ice model experiments to show that the diagnosed patterns of sea surface height (SSH) anomalies associated with changes in the MOC in the North Atlantic (NA) depend critically on the time scales of interest. Model hindcast simulations for 1958-2004 reproduce the observed pattern of SSH variability with extrema occurring along the Gulf Stream (GS) and in the Subpolar Gyre (SPG), but also show that the pattern is primarily related to the wind-driven variability of MOC and gyre circulation on interannual time scales; it is reflected also in the leading EOF of SSH variability over the NA ocean as described in previous studies. The pattern is, however, not useful as a "fingerprint" of longer-term changes in the MOC: as shown with a companion experiment, a multi-decadal, gradual decline in the MOC (of 5Sv over 5 decades) induces a much broader, basin-scale SSH rise over the mid-to-high-latitude NA, with amplitudes of 20cm. The detectability of such a trend is low along the GS since low-frequency SSH changes are effectively masked here by strong variability on shorter time scales. More favorable signal-to-noise ratios are found in the SPG and the eastern NA where a MOC trend of 0.1Sv/yr would leave a significant imprint in SSH already after about 20 years.

1. Introduction

Global climate model simulations suggest the possibility of a gradual decline of the meridional overturning circulation (MOC) in the Atlantic Ocean during the 21st century [*Meehl et al.*, 2007; *Gregory et al*., 2005]. The projected reductions due to anthropogenic warming and freshening in the northern North Atlantic (NA) range from 0 to about 50%, not including possible additional effects due to enhanced melting of the Greenland ice sheet [*Jungclaus et al*., 2006]. Since the strength of the MOC is intimately linked to the meridional transport of heat [*Biastoch et al.*, 2008; *Rhines et al.,* 2008] and also affects the sequestration of carbon dioxide [*Sarmiento and LeQuéré*, 1996; *Biastoch et al.*, 2007] in the NA Ocean, a progressive weakening is expected to have major implications for the future evolution of climate [*Bindoff et al*., 2007], particularly for Northwest Europe [*Vellinga and Wood*, 2002].

The detection of a gradual change in the MOC is a challenging task for ocean observing systems, involving the determination of trends in meridional velocity fields along transoceanic sections that are characterized by strong variability over a broad spectrum of space and time scales. Observational efforts have focused on the subtropical NA, particularly along 26.5°N where the presence of a well-defined western boundary current together with the structure of the interior temperature and salinity fields permits a determination of the MOC and the associated heat transport from individual hydrographic surveys to an accuracy of ±15-20% [*Bryden and Imawaki,* 2001]. While historical occupations of this section, i.e., the five repeats between 1957 and 2004 [*Bryden et al.,* 2005], are considered too infrequent to avoid an aliasing of high-frequency variability in the calculation of long-term trends [*Baehr et al., 2007*; *Wunsch,* 2008], the monitoring system established by the RAPID/MOCHA effort in March 2004 [*Marotzke et al.,* 2002] has begun to provide a continuous record of the MOC transport at this latitude. However, the presence of vigorous variability on intra-seasonal to

interannual time scales [*Cunningham et al.,* 2007*; Kanzow et al.,* 2007] still poses a formidable challenge for the detection of long-term changes in the MOC, suggesting that continuous measurements over multi-decadal time spans (>60 years for an assumed observation error of 1Sv) are required to detect a trend of the magnitude projected by the IPCC model results [*Baehr et al.,* 2007].

Since the MOC is reflected in the near-surface current fields, e.g., in the strength and position of the GS and North Atlantic Current (NAC), an important indirect indicator of MOC changes could be provided by regional patterns of sea surface height (SSH) anomalies associated with the dynamic adjustment of surface circulation features. Model studies noted that variability of the MOC is associated with pronounced regional changes in SSH especially in the western NA [*Bryan*, 1996; *Häkkinen*, 2000], typically being characterized by a dipole (or, tripole) pattern of changes centered in the subpolar gyre (SPG) and along the GS/NAC, with weaker changes in the subtropical gyre (STG). A similar pattern was found in relation to interannual-to-decadal MOC variability in the leading empirical orthogonal function (EOF) of SSH anomalies simulated by a 1000-year climate model control run by *Zhang* [2008], suggesting its potential use as a "fingerprint" of MOC strength. Modelling studies arrived at conflicting results, however, concerning the manifestation of long-term MOC trends in regional SSH patterns: while dynamic sea level change in an IPCC-scenario run projecting a MOC decline of 25% was characterized by a similar dipole/tripole as above [*Landerer et al*., 2007], the simulation of a major MOC decline by *Levermann et al*. [2005] showed a very different pattern, with a much broader, basin-scale sea level rise over most of the NA.

In the study presented here we use a sequence of ocean model experiments to demonstrate that in order to rationalize regional patterns of SSH anomalies and their association with

MOC changes in the NA, it is of first importance to distinguish variability on interannual-to-decadal time scales from longer-term changes.

2. Model Experiments

Our aim is to examine the manifestation in regional dynamic SSH patterns of a multi-decadal decline in the MOC, and to contrast these patterns with the natural SSH variability patterns on intra-seasonal to decadal time scales due to atmospheric forcing and internal dynamic processes. Our modelling strategy is based on a sequence of global model experiments, involving a set of hindcast simulations (with and without eddies permitted) forced by atmospheric reanalysis products for 1958 to 2004, and a perturbation experiment in which the MOC is artificially forced to decline by imposing freshwater flux anomalies in the northern NA. The model experiments are based on different implementations of NEMO [*Madec,* 2006], involving coupled ocean (OPA9)-sea ice (LIM2) models in global-grid configurations (ORCA) at ½° resolution (ORCA05; the grid spacing in the mid-latitude NA is about 40km) developed as part of the DRAKKAR collaboration [*The DRAKKAR Group*, 2007]. The model uses 46 levels in the vertical; the bottom cells are allowed to be partially filled. The effect of explicitly simulated mesoscale eddies was assessed by a companion study with an eddy-permitting (¼°) configuration (ORCA025; *Barnier et al.* [2006]). While showing a somewhat (~20%) stronger intraseasonal-to-interannual MOC variability than CNTRL, it indicated relatively minor effects of eddy dynamics on the concomitant, large-scale SSH patterns dicussed in this paper. A presentation of results from the eddying model case is thus deferred to the supplementary material (Figures S1-S4).

The surface boundary conditions use the formulations and data sets developed by *Large and Yeager* [2004] that have been taken as the basis for the "Co-ordinated Ocean-ice Reference

105 Experiments" (COREs) proposed by *Griffies et al.* [2008]. The 6 hourly (wind, humidity, air
106 temperature), daily (short and long wave radiation) and monthly (freshwater fields) forcing
107 data consist of a combination of NCEP/NCAR reanalysis products [*Kalnay et al.*, 1996] with
108 various satellite data sets, and involve corrections for global imbalances. Turbulent fluxes are
109 computed from bulk formulae as a function of the prescribed atmospheric state and the
110 simulated ocean surface state. The spurious salinity drifts typically occurring under such
111 conditions [cf. *Griffies et al.*, 2008] are minimized by a relaxation of salinity to climatological
112 conditions, adopting two different configurations: both versions use a "weak restoring" (with
113 time scales of 180 and 360 days) of sea surface salinity (SSS) over the bulk of the domain; for
114 the polar oceans one version uses an enhanced restoring (time scale of 1 month) of SSS, the
115 other version uses a "weak" (180 days) relaxation of salinity for the whole water column (as
116 used before by *Biastoch et al.* [2008]). Comparison of experiments with different restoring
117 configurations showed little effects on the SSH variability patterns, i.e., confirmed that the
118 solution behaviors considered in this study are robust with respect to this aspect of the model
119 configuration.
120
121 The main set of experiments consists of a hindcast simulation (CNTRL) of the atmopherically
122 forced variability for 1958-2004, and a perturbation experiment (FRESH) in which a decline
123 in the MOC is artificially induced by a 15% to 20% increase of precipitation in the northern
124 NA (corresponding to a zonal average of 0.15m/yr or 0.08Sv surplus in the freshwater flux).
125 The imposed change in the freshwater budget leads to a declining trend in the MOC transport
126 by about 5Sv over the duration of the experiment (Figure 1), without a substantial change in
127 the vertical structure: Annual mean differences between CNTRL and FRESH of the stream
128 function of meridional transport in years 1970 and 2000 show a weakening of the stream
129 function, while its general structure, with its mid-latitude maximum at about 1000m depth,

remains largely the same (not shown). The magnitude of the (artificially induced) trend is reminiscent of the MOC behavior in global warming scenarios as discussed in *Gregory et al.* [2005]. Note that despite the differences in the trends, the MOC variability is almost identical in the two runs, demonstrating the prime importance of the surface heat and momentum fluxes for the variability on interannual-to-decadal time scales as discussed by *Biastoch et al.* [2008]. For a test of the robustness of the SSH signatures, and an assessment of their dynamical causes, we have included two additional experiments: a sensitivity experiment (CNTRL-GM) in which eddy effects were parameterized following *Gent and McWilliams* [1990]; and a corresponding perturbation experiment with this configuration (WIND-GM) which aimed at identifying the individual role of wind stress variability by using annually repeating seasonal climatologies for the heat and freshwater fluxes.

For the time tendency of dynamic changes of SSH, η, the model uses a prognostic (implicit time-stepping) free surface formulation

$$\frac{\partial \eta}{\partial t} = -\nabla_h \cdot \vec{U} - q_w$$

$$\vec{U} = \int_{-H}^{\eta} \vec{u}_h dz \quad \text{and} \quad \eta = \bar{\eta} + \eta_d$$

where H is the ocean depth, $\vec{u}$ is the horizontal velocity and q_w is the net surface freshwater flux. In our analysis we follow previous studies [*Landerer et al.,* 2005; *Wunsch et al.,* 2007] and subtract a globally uniform, but time-varying value, $\bar{\eta}$, which reflects the net expansion/contraction of the global ocean [*Greatbatch*, 1994] but has no dynamical impact. We refer to the adjusted sea level as *dynamic SSH*, η_d. As observational reference we use a gridded (⅓°x ⅓° Mercator) product of 7-day averages of satellite altimeter SSH anomalies

with respect to a several-year mean from which we also subtracted a global mean value [cf. *Wunsch et al*., 2007].

3. Assessment of mid-latitude circulation variability

While the realism of the simulated MOC variability cannot be tested directly, observational records allow some assessment of the associated changes in the mid-latitude circulation. A metric of prime importance for inspecting changes over the last five decades is provided by the index of baroclinic transport between Bermuda and the Labrador Sea proposed by *Curry and McCartney* [2001; hereafter CM-index] which reflects changes in the GS/NAC transport in the upper 2000m (Figure 2a). The hindcast simulations (CNTRL and CNTRL-GM) capture the observed rise of the CM-index from weak transports in the early 1970s to a maximum in the mid-1990s, and the subsequent decline to a minimum in 2001-2002; correlations with the observed index are 0.77 for both CNTRL and CNTRL-GM. The main departure from the observed CM-index, and between the two hindcasts, lies in the amplitude of decadal variations (especially with regard to the transport maximum in the mid-1990s) which appears to be sensitive to model parameterization choices, i.e., GM vs. not GM. (Note that the companion, eddy-permitting model run shows a similar decadal behavior like CNTRL-GM after a spin-up of ten years with similar amplitude (see supplementary Figure S2)).

Changes in the intensity of the SPG are reflected in altimeter observations of SSH anomalies. A useful SPG-index [*Häkkinen and Rhines*, 2004; *Hátún et al.*, 2005] is provided by the principal component of an EOF-analysis of η_d, or alternatively, by η_d in the center of the Labrador Sea where the cyclonic circulation is associated with a depression in mean sea level. A comparison of CNTRL with the observed time series of η_d in the central gyre is shown in Figure 2b. A main signal in both is the rise by 8cm between 1993 and 1999 that corresponds

177 to a sharp decline in the SPG strength, with a partial recovery thereafter [*Böning et al.*, 2006].
178 We note that over such a short period the simulated η_d in FRESH is not significantly
179 different: it is only for time spans longer than ~15 years that the trend in FRESH becomes
180 manifest; over five decades the MOC decline in that case leads to a rise in η_d of about 20cm.
181
182 **4. Spatial pattern of interannual-to-decadal SSH variability**
183 Having established the model's fidelity in simulating observational indices of mid-latitude
184 circulation variablity, we now examine the spatial η_d variability patterns. We begin by
185 assessing the simulated signatures with satellite altimeter data since 1993, before proceeding
186 to the question of the manifestation of MOC changes on different time scales. The standard
187 deviation of η_d over the period 1993-2004 in CNTRL is characterized by a similar
188 distribution as in the observations (Figure 3): highest amplitudes are associated with major
189 frontal regions such as the GS/NAC (and the Malvinas Current/Zapiola anti-cyclone in the
190 South Atlantic), suggesting that the interannual variability of η_d is concentrated in the same
191 regions as the high-frequency variability, and thus reminiscent of the distribution of eddy
192 variability in the Atlantic Ocean [e.g. *Fu and Smith*, 1996].
193
194 The spatial distribution in the mid-latitude NA of the changes in η_d during the 1990s has
195 been analysed in several studies, and described as a basin-wide coherent dipole structure
196 between the subpolar and subtropical NA; it changed sign between 1995 and 1996 in response
197 to a sharp drop in the North Atlantic Oscillation (NAO) index [*Esselborn and Eden*, 2001;
198 hereafter *EE01*]. The dipole (or rather, tripole) pattern is clearly exhibited by the linear trend
199 of η_d in the mid-latitude NA during 1993-1999 (Figure 4a), the period of the strong decline in
200 the SPG-index (Figure 2b): η_d-changes are positive in the SPG, while negative values

dominate along the path of the GS/NAC and in turn, weak positive values in the STG. The main observed features are already well reproduced in the hindcast simulations at ½° resolution (Figure 4); the eddy-permitting (¼°) simulation exhibits an increased fidelity in reproducing smaller-scale features like the SSH variations in the Northwest Corner as well as along the GS/NAC path (see suppl. material). In contrast, the adoption of GM-mixing (Figure 4b,d) which effectively suppresses the generation of mesoscale eddies in the ¼°-case, leads to smoother patterns than in CNTRL (Figure 4c). From the comparable set of simulations we can conclude that the model captures the salient aspects of the decadal circulation variability in the mid-latitude NA.

This level of skill is also exhibited by an EOF analysis of (detrended) η_d time series, where the leading mode for 1993 to 2004 in CNTRL is almost indistinguishable from the observational pattern for this period (Figure 5), explaining in both cases 31% of the variance. Note that the EOF patterns and amplitudes of FRESH of the original η_d time series during the 1990s are very similar to CNTRL, although the MOC in that case has weakened by 50%: it gives a first indication that this pattern is related to interannual circulation changes and not much influenced by longer-term trends. Over the extended period of the model simulation, i.e. from 1958 to 2004, the first EOF (Figure 6) explains 22% of the variance and exhibits a large-scale pattern of alternating changes in the SPG (north of ~40°N), mid-latitudes (~25°-40°N), and tropical NA that matches the results discussed in previous studies [e.g. *Häkkinen*, 2001, *Häkkinen and Rhines*, 2004; *Zhang*, 2008].

A question of interest in the present study is whether this η_d-pattern can be attributed to buoyancy-driven, large-scale MOC changes in the North Atlantic or whether it is due to other dynamical causes. The dynamic nature of the SSH variability signal during the 1990s has

226 been attributed by *EE01* to a re-distribution of upper-ocean heat content associated with a fast
227 dynamical response of the circulation to a drop in NAO-index in the mid-1990s. Idealized
228 model experiments [*EE01*; *Eden and Willebrand*, 2001] suggested a primary role of the wind
229 stress in inducing SSH anomalies on time scales of a few years. These findings are confirmed
230 and extended by experiment WIND-GM: the purely wind-driven changes in η_d during 1993-
231 1999 (Figure 4c) suffice to reproduce the large-scale pattern of the reference solution over the
232 whole Atlantic Ocean (Figure 4b); the same is true for the leading EOF of the wind-driven
233 variability over the whole simulation period 1958-2004 (Figure 6).
234
235 **5. SSH pattern related to a multi-decadal MOC decline**
236 In contrast to the alternating η_d-pattern related to interannual-to-decadal variability of the
237 wind stress, a distinctly different distribution emerges as a result of the multi-decadal MOC
238 decline simulated in FRESH: the η_d-trend in that case (Figure 7) shows a rise in sea level
239 over the whole NA, with a broad maximum of about 5mm/yr spanning the SPG and parts of
240 the NAC, contrasted by somewhat weaker decreases of 2mm/yr in the southern hemisphere.
241 The dominant feature of the η_d-change after five decades of MOC decline is thus a positive
242 south-north gradient of about 20cm in the Atlantic Ocean, reflecting a pronounced
243 interhemispheric mass redistribution, as in the climate modelling results of *Levermann et al.*
244 [2005]. An interesting regional-scale feature that was also noted in recent studies of IPCC-
245 scenario runs by *Yin et al.* [2009] and *Hu et al.* [2009], is the wedge of rising sea levels that
246 extends southward from the SPG along the American coast to about 35°N.
247
248 The simulated η_d-trend pattern in FRESH (Figure 7) is very similar to the leading EOF
249 pattern of the unfiltered (no temporal linear trend removed) annual mean η_d-variability. By

250 explaining 67% of the variance in the NA, it is clearly the dominant pattern of multi-decadal
251 variability of η_d in this experiment. A statistical comparison of the unfiltered multivariate
252 η_d-variability between WIND-GM and FRESH, following the methodology of *Dommenget*
253 [2007], confirms that the pattern related to the MOC-trend differs significantly from the
254 pattern of wind-driven variability. The structure of the MOC-related η_d-trend in FRESH
255 reflects a weakening of the eastward currents in the northern/southern mid-latitudes, The
256 weakening of the NAC is consistent with the declining CM-index seen in Figure 2a; it also
257 indicates an overall weakening of the SPG, and a weaker STG circulation in the eastern NA
258 (i.e., weaker Canary Current and North Equatorial Current).
259
260 Having established the η_d-signatures of a multi-decadal MOC decline, we now turn to
261 address the issue of its detectability in the real ocean: more specifically, can the signature of a
262 gradual MOC-related trend be detected against the presence of higher-frequency "noise"
263 associated with wind-driven and internal dynamic processes? We first assess the
264 manifestation of MOC-variability in regional SSH changes by examining the linear regression
265 of η_d onto the MOC-transport at 26°N in FRESH (Figure 8a). Maximum regression values of
266 -4.5cm/Sv (significant at the 95% level) are found in the SPG and also along the West
267 European coast. The distribution is reminiscent of previous findings obtaines from a different
268 (coarse-resolution climate) model and approach by *Levermann* et al. [2005].
269
270 To determine if these regression patterns are primarily caused by the interannual variability or
271 the trend of the MOC, we computed the percentage of the trend-induced contribution to the
272 covariance. The relative contribution of a linear trend (signal) and internal variability (noise)
273 to the SSH-MOC regression is obtained by utilizing symmetry properties for the covariance
274 of two variables [*von Storch and Zwiers,* 1999]: by decomposing the complete covariance into

the sum of the covariances of the linear trends and of the deviations (residuals) from the trends, a percentage expression for the trend-induced covariance

$$r_{trend} = \frac{\left\|\mathrm{cov}(trend(x_1), trend(x_2))\right\|}{\left\|\mathrm{cov}(x_1' x_2')\right\| + \left\|\mathrm{cov}(trend(x_1), trend(x_2))\right\|} \mathrm{x}100$$

is obtained, where x_1 and x_2 stand for the two time series and the prime for the point-wise temporal trend-removed time series.

Based on this analysis we can identify the regions where the relative impact of the long-term MOC change dominates the η_d -variability in FRESH (Figure 8b): particularly high values are found for a "horseshoe" pattern with maxima of >80% from the SPG along the West European coast. The long-term MOC trend manifests itself also (with values above 50%) along the in-shore side of the GS, consistent with recent results of *Hu et al.* [2009]. In contrast, the trend contribution is below 50% along the off-shore side of the GS, implying that this region is not a sensitive indicator for long-term MOC changes.

Having determined where a significant MOC-imprint can be expected, the question remains: after what observation period could such a trend be detected against the background of high-frequency (intral-seasonal-to-interannual) SSH variability? To assess the significance of a trend signal we use the *t*-test [e.g. *von Storch and Zwiers,* 1999]:

$$r_{x_1,t} = \pm \frac{T(N)}{\sqrt{T^2(N) + N(t)}}$$

which determines the correlation *r* between a time series x_1 and the time *t* in terms of the ratio of *T* (critical value from the *t*-distribution) and the number of the degrees of freedom *N* (the number of independent samples). We estimate *N* by the time lag at which the autocorrelation function of η_d in CNTRL drops below 0.2: it gives periods of 3.5 years for the Labrador Sea,

298 4.5 for the SPG, 7 years for a "West European" box, and 2.5 years for two boxes along the
299 North American coast, respectively (for the definition of the boxes see Figure 8b). From this
300 we obtain minimum time periods for a significant detection (at the 95% level) of the trend
301 signal in FRESH of 16 years for the SPG and 24 years for the West European box; in contrast,
302 a significant trend detection based on the SSH-changes along the North American coast
303 would require periods longer than the model integration time of 47 years. It is interesting to
304 note, that the detection times are not significantly affected by the box sizes, e.g., there is only
305 little difference between the estimates for the SPG box and the single station point in the
306 center of the Labrador Sea. An application to the real ocean would, in addition, need to
307 account for SSH-measurement errors; more specifically, the detection periods would increase
308 to 19 years (SPG) and 31 years (West European box) by assuming an altimeter measurement
309 uncertainty of 2cm.
310
311 **6. Concluding discussion**
312 The model study suggests repercussions of a gradual decline (in this study: of 5Sv over five
313 decades) in MOC strength on SSH anomaly fields that are in marked contrast to the dipole
314 pattern of interannual SSH anomalies described in previous studies. Our analysis shows that
315 the latter signature, with strongest SSH anomalies along the GS and NAC, can be attributed
316 mainly to the response of ocean circulation to changes in wind stress. In contrast, the
317 dynamical impact on SSH of a longer-term trend in the MOC associated with a decline in
318 subarctic deep water formation, is a broad SSH rise in the NA and a broad SSH fall in the
319 southern hemisphere. A similar interhemispheric seasaw has been reported in coarse-
320 resolution climate model runs and rationalized in terms of a large-scale redistribution of mass,
321 i.e. an adiabatic adjustment in the ocean's density structure [*Levermann et al.*, 2005].
322

323 The difference in SSH patterns suggests that over the mid-latitude NA, the manifestation of
324 changes in MOC transport critically depends on the time scales of interest. A general
325 implication is that trend studies of SSH patterns based on available, relatively short (13-year)
326 altimeter records [*Bindoff et al.*, 2007; *Cromwell et al.*, 2007; *Polito and Sato*, 2008] have to
327 be interpretated with caution, especially along the GS in the mid-latitude western North
328 Atlantic where the SSH variability is dominated by strong intra-seasonal-to-interannual
329 fluctuations. Because of this intense, high-frequency "noise" in SSH time series, the
330 manifestation of a gradual trend in the MOC would effectively be masked in the GS regime.
331 In this regard our ocean model analysis challenges previous conclusions drawn from coarse-
332 resolution climate model simulations which suggested a significant imprint of a possible
333 future MOC decline on sea level trends along the North American coast [*Hu et al.*, 2009].
334
335 A much more favorable signal-to-noise ratio of a long-term MOC trend is found in the SPG
336 and eastern NA, suggesting that an index of SSH changes in these regions could potentially
337 provide a valuable contribution to an effective MOC-monitoring system. More specifically,
338 our model results suggest that a 0.1Sv/yr-decline in the MOC strength (a rate similar to
339 projections from IPCC-climate-scenario simulations for the 21st century) corresponds to an
340 SSH anomaly signal that would stand out against the high-frequency, primarily wind-driven
341 and internally generated (eddy) noise after about 20-30 years in the SPG and eastern NA. This
342 time scale also implies that if changes in the MOC were underway already as suspected in
343 some studies [B*ryden et a*l., 2005], it should only be a few years before the record of altimeter
344 observations of SSH would cross the threshold for detectability of such a trend.

Acknowledgements

This work was supported by the Deutsche Forschungsgemeinschaft in the framework of Schwerpunktprogramm 1257 *Massentransporte und Massenverteilungen im System Erde* and by the Bundesministerium für Bildung und Forschung (BMBF)-Verbundprojekt *Nordatlantik*. The ocean model integrations were performed at the computing centers of Kiel University and the Norddeutscher Verbund für Hoch- und Höchstleistungsrechnern (HLRN). We thank the NEMO System Team and the DRAKKAR Group for the technical support during all stages of the model set up and integration as well as Johannes Karstensen for his valuable and helpful comments on the model analysis. The altimeter products were produced by Ssalto/Duacs and distributed by AVISO, with support from CNES and available via ftp://ftp.cls.fr/pub/oceano/AVISO/SSH/duacs/global/dt/ref/msla/merged/h.

References

Barnier, B., and Coauthors, 2006: Impact of partial steps momentum advection schemes in a global ocean circulation model at eddy-permitting resolution, *Ocean Dynamics*, **56**, doi: 10.1007/s10236-006-0082-1.

Baehr, J., K. Keller, and J. Marotzke, 2007: Detecting potential changes in the meridional overturning circulation at 26°N in the Atlantic, *Climate Change*, doi:10.1007/s10584-006-9153-z.

Biastoch, A., C. Völker, and C.W. Böning, 2007: Uptake and spreading of anthropogenic C02 in an eddy-permitting model of the Atlantic Ocean, *J. Geophys. Res.,* **112**, C09017, doi:10.1029/2006JC003966.

Biastoch, A, C.W. Böning, J. Getzlaff, J.-M. Molines, and G. Madec, 2008: Mechanisms of interannual - decadal variability in the meridional overturning circulation of the mid-latitude North Atlantic Ocean, *J. Climate*, **21**, doi: 10.1175/2008JCLI2404.1.

Bindoff, N.L., and Coauthors, 2007: Observations: Oceanic Climate Change and Sea Level. In: *Climate Change 2007: The Physical Science Basis. Contribution of Working Group I to the Fourth Assessment Report of the Intergovernmental Panel on Climate Change* (S. Solomon et al. [eds.]), Cambridge University Press, 385-432.

Böning, C.W., M. Scheinert, J. Dengg, A. Biastoch, and A. Funk, 2006: Decadal variability of subpolar gyre transport and its reverberation in the North Atlantic overturning, *Geophys. Res. Lett.*, **33**, L21S01, doi: 10.1029/2006GL026906.

Bryan, K., 1996: The steric component of sea level rise associated with enhanced greenhouse warming: a model study, *Climate Dynamics*, **12**, 545-555.

Bryden, H.L., and S. Imawaki, 2001: Ocean heat transport. In: *Ocean Circulation and Climate*, (G. Siedler et al.[eds.]), Academic Press, 455-474.

Bryden, H. L., H.R. Longworth, and S.A. Cunningham, 2005: Slowing of the Atlantic meridional overturning circulation at 25°N, *Nature*, **438**, doi:10.1038/nature04385.

Cromwell, D., A.G.P. Shaw, P. Challenor, R.E. Houseago-Stokes, and R. Tokmakian, 2007: Towards measuring the meridional overturning circulation from space, *Ocean Sci.*, **3**, 223-228.

Cunningham, S.A., T. Kanzow, D. Rayner, M.O.Barringer, W.E. Johns, J. Marotzke, H.R. Longworth, E.M. Grant, J.J.-M. Hirschi, L.M. Beal, C.S. Meinen and H. Bryden, 2007: Temporal Variability of the Atlantic Meridional Overturning Circulation at 26.5°N, *Science*, **317**, doi:10.1126/science.1141304.

Curry, R.G., and M.S. McCartney, 2001: Ocean gyre circulation changes associated with the North Atlantic oscillation, *J. Phys.Oceanog*., **31(12)**, 3374-3400.

Dommenget, D., 2007: Evaluating EOF modes against a stochastic null hypothesis, *Climate Dynamics*, *28*, doi:10.1007/s00382-006-0195-8.

DRAKKAR Group, the: B. Barnier, L. Brodeau, J. Le Sommer, J.-M Molines, T. Penduff, S. Theetten, A.-M. Treguier, G. Madec, A. Biastoch, C. Böning, J. Dengg, S. Gulev, R. Bourdallé Badie, J. Chanut, G., Garric, S. Alderson, A. Coward, B. de Cuevas, A. New, K. Haines, G. Smith, S. Drijfhout, W. Hazeleger, C. Severijns, P. Myers, 2007: Eddy-Permitting Ocean Circulation Hindcasts of Past Decades, *Clivar Exchanges*, **12**, 8-10.

Eden, C., and J. Willebrand, 2001: Mechanism of interannual to decadal variability of the North Atlantic circulation , *J. Climate*, **14(10)**, 2266-2280.

Esselborn, S., and Eden, C., 2001: Sea surface height changes in the North Atlantic ocean related to the North Atlantic Oscillation, *Geophys. Res. Lett*, **28(18)**, 3473-3476.

Fu, L., and R. Smith, 1996: Global ocean circulation from satellite altimetry and high-resolution computer simulation, *Bull. Am. Meteorol. Soc*., **77**, 2625-2636.

404 Gent, P. R., and J. C. McWilliams, 1990: Isopycnal mixing in ocean circulation models, *J.*
405 *Phys. Oceanogr.*, **20**, 150–155.
406 Greatbatch, R., 1994: A note on the representation of steric sea level in models that
407 conserve volume rather than mass, *J. Geophys. Res.*, **99(C6)**, 12,767-12,771.
408 Gregory, J. M., et al., 2005: A model intercomparison of changes in the Atlantic
409 thermohaline circulation in response to increasing atmospheric $C0_2$ concentration, *Geophys.*
410 *Res. Lett*., **32**, L12703, doi:10.1029/2005GL023209.
411 Griffies, S., and Coauthors, 2009: Coordinated Ocean-ice Reference Experiments
412 (COREs), *Ocean Modelling,* **26**, 1-2, 1-46, doi:10.1016/j.ocemod.2008.08.007.
413 Häkkinen, S., 2000: Decadal Air–Sea Interaction in the North Atlantic Based on
414 Observations and Modeling Results, *J. Climate*, **13**, 1195–1219.
415 Häkkinen, S., 2001: Variability in the sea surface height: A qualitative measure for the
416 meridional overturning in the North Atlantic, *J. Geophys. Res*., **106(C7)**, 13,837-13,848.
417 Häkkinen, S., and P.B. Rhines, 2004: Decline of Subpolar North Atlantic Circulation
418 During the 1990s, *Science*, **304**, doi:10.1126/science.1094917.
419 Hátún, H., A.B. Sandø, H. Drange, B. Hansen and H. Valdimarsson, 2005: Influence of the
420 Atlantic Subpolar Gyre on the thermohaline circulation, *Science*, **309**, 1841-1844.
421 Hu, A., G.A. Meehl, W. Han, and J. Yin, 2009: Transient response of the MOC and
422 climate to potential melting of the Greenland Ice Sheet in the 21st century, *Geophys. Res.*
423 *Lett.*, **36**, L10707, doi:10.1029/2009GL037998.
424 Jungclaus, J. H., H. Haak, M. Esch, E. Roeckner, and J. Marotzke, 2006: Will Greenland
425 melting halt the thermohaline circulation?, *Geophys. Res. Lett*., **33**, L17708,
426 doi:10.1029/2006GL026815.
427 Kalnay, E., and Coauthors, 1996: The NCEP/NCAR 40-Year Reanalysis Project, *Bull.*
428 *Amer. Meteor. Soc*, **77**, 437-471.

Kanzow, T., S.A. Cunningham, D. Rayner, J.J.-M. Hirschi, W.E. Johns, M.O. Baringer, H.L. Bryden, L.M. Beal, C.S. Meinen, and J. Marotzke, 2007: Observed Flow Compensation Associated with the MOC at 26.5°N in the Atlantic, *Science*, **317,** doi:10.1126/science.1141293.

Landerer, F.W., J.H. Jungclaus, and J. Marotzke, 2007: Regional Dynamic and Steric Sea Level Change in Response to the IPCC-A1B Scenario, *J. Phys. Oceanogr.*, **37**, doi:10.1175/JPO3013.1.

Large, W. and S. Yeager, 2004: Diurnal to decadal global forcing for ocean and sea-ice models: the datasets and flux climatologies. *NCAR Technical Note*: NCAR/TN-460+STR, CGD Division of the National Centre for Atmospheric Research.

Levermann, A., A. Griesel, M. Hoffmann, M. Montoya, and S. Rahmstorf, 2005: Dynamic sea level changes following changes in the thermohaline circulation, *Climate Dynamics*, **24,** doi:10.1007/s00382-004-0505-y.

Madec, G., 2006: NEMO: the OPA ocean engine, *Note du Pole de Modelisation*, 110pp.

Marotzke, J., S.A. Cunningham, and H.L. Bryden, 2002: Monitoring the Atlantic meridional overturning circulation at 26.5°N. Available at: http://www.soton.ac.uk/rapidmoc.

Meehl, G.A., and Coauthors, 2007: Global Climate Projections. In: *Climate Change 2007: The Physical Science Basis. Contribution of Working Group I to the Fourth Assessment Report of the Intergovernmental Panel on Climate Change* (S. Solomon et al. [eds.]), Cambridge University Press, 747-845.

Polito, P.S., and O.T. Sato, 2008: Global Interannual Trends and Amplitude Modulations of the Sea Surface Height Anomaly from the TOPEX/*Jason-1* Altimeters, *J. Climate,* **21**, doi: 10.1175/2007JCLI1924.1.

452 Rhines, P., Häkkinen, S., and Josey, 2008: Is oceanic heat transport significant in the
453 climate system? In: *Arctic-Subarctic Ocean Fluxes* (Dickson, R.R., J. Meincke and P. Rhines
454 [eds.]), Springer Netherlands, 87-109, doi:10.1007/978-1-4020-6774-7.
455 Sarmiento, J.L., and C. LeQuéré, 1996: Oceanic carbon dioxide uptake in a model of
456 century-scale global warming, *Science*, **27**, 1346-1350.
457 Storch, von, H., and F.W. Zwiers, 1999: *Statistical Analysis in Climate Research*, doi:
458 10.2277/0521012309.
459 Vellinga, M., and R.A. Wood, 2002: Global climate impacts of a collapse of the Atlantic
460 Thermohaline Circulation, *Climatic Change*, **54**, 251-267.
461 Wunsch, C., R.M. Ponte, and P. Heimbach, 2007: Decadal Trends in Sea Level Patterns:
462 1993-2004, *J. Climate*, *27*, doi: 10.1175/2007JCLI1840.1.
463 Wunsch, C., 2008: Mass and volume transport variability in an eddy-filled ocean, *Nature*
464 *Geoscience*, **1**, 165-168, doi:10.1038/ngeo126.
465 Yin, J., M. E. Schlesinger, and R. J. Stouffer, 2009: Model projections of rapid sea-level
466 rise on the northeast coast of the United States, *Nature Geoscience*, **2**, 262-266, doi:
467 10.1038/NGEO462.
468 Zhang, R., 2008: Coherent surface-subsurface fingerprint of the Atlantic meridional
469 overturning circulation, *Geophys. Res. Lett*., **35**, L20705, doi:10.1029/2008GL035463.

Figures

Figure 1. Indices of large-scale transport variability. Maximum of the stream function of zonally integrated volume transport (MOC-transport) at 26.5°N in CNTRL and FRESH: monthly mean values (thin lines) and interannually-smoothed with a 23-month Hanning filter (bold lines). Shading is relative to the long-term (1958-2004) linear trends (straight lines). Dashed lines mark ± one standard deviation of annual mean anomalies. The simulations exhibit similar variability relative to the trends, with correlations of 0.98 for monthly and 0.84 for smoothed values.

Figure 2. Indices of large-scale transport variability. (a) Index of observed (red) annual mean baroclinic mass transport anomaly between the subpolar and subtropical gyres following *Curry and McCartney* [2001] in comparison to the model simulations CNTRL (green) and CNTRL-GM (black), whereby the amplitude of year-to-year variability amounts to 5.0Sv in the observations, 1.8Sv in CNTRL and 3.8Sv in CNTRL-GM. **(b)** Subpolar gyre index following *Häkkinen and Rhines* [2004] and *Hátún et al.* [2005] as given by the annually smoothed monthly mean sea level anomaly η_d at 57°N, 52°W in AVISO satellite altimeter data (red), CNTRL (green) and FRESH (blue), with linear trends (solid) and standard deviations of interannual variability (dashed). Note, that the climatological seasonal cycle over the period shaded in grey has been subtracted, resulting in a shift of these "normalized" time series to emphasize the similarity of interannual variability of both model cases and observational data.

493 **Figure 3. Interannual sea level variability: Model vs. altimeter data.** Standard deviation
494 during 1993 to 2004 of annual mean anomalies of dynamic SSH, η_d (in cm): **(a)** AVISO data
495 and **(b)** CNTRL.
496
497 **Figure 4. Interannual sea level trend: Model vs. altimeter data.** Linear trend (1993-1999)
498 of η_d (in mm/yr) in comparison between **(a)** AVISO data and simulations: **(b)** CNTRL, **(c)**
499 WIND-GM and **(d)** CNTRL-GM.
500
501 **Figure 5. Patterns of interannual sea level variability.** First EOF of detrended anomalous
502 annual means of η_d over the observational period (1993-2004) in **(a)** AVISO data and **(b)**
503 CNTRL.
504
505 **Figure 6. Dynamic cause of interannual sea level variability patterns.** First EOF of
506 detrended anomalous annual means of η_d over the hindcasting period (1958-2004) in **(a)**
507 CNTRL-GM and **(b)** WIND-GM.
508
509 **Figure 7. SSH changes due to multi-decadal MOC decline.** Linear trend (1958-2004) of
510 η_d (in mm/yr) in FRESH relative to CNTRL.
511
512 **Figure 8. Manifestation of multi-decadal MOC decline. (a)** Linear regression (1958-2004)
513 of anomalous annual mean η_d and the MOC-index in FRESH (in cm/Sv); grey areas indicate
514 non-significant values at the *t*-test 95% level **(b)** Percentage of the covariance between local
515 η_d and the MOC-index due to the linear trends in both variables. Boxes indicate regions
516 where we have assessed the detectability of a gradual MOC decline as simulated in FRESH

based on continuous records of η_d (Labrador Sea: 57°N/52°W; SPG: average from 45°-60°N and 30°-50°W, "West European" box: average from 35°-45°N and 12°-22°W, and two sites along the North American coast: 41°-43°N/65°-68°W and 45-46°N/56°-58°W).

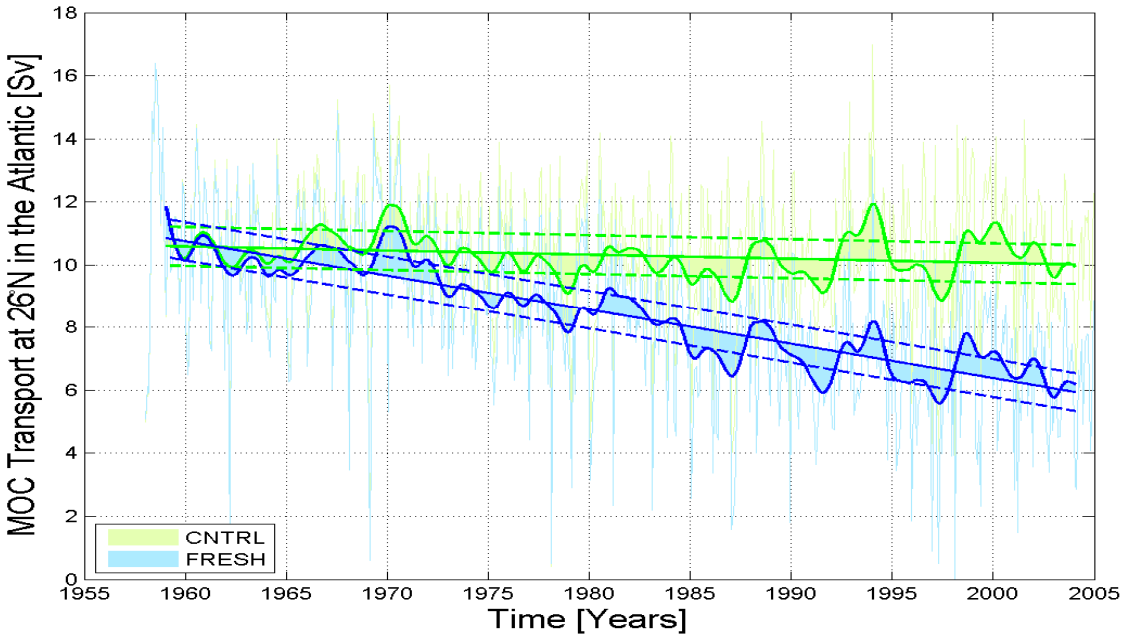

Figure 1. Indices of large-scale transport variability. Maximum of the stream function of zonally integrated volume transport (MOC-transport) at 26.5°N in CNTRL and FRESH: monthly mean values (thin lines) and interannually-smoothed with a 23-month Hanning filter (bold lines). Shading is relative to the long-term (1958-2004) linear trends (straight lines). Dashed lines mark +/- one standard deviation of annual mean anomalies. The simulations exhibit similar variability relative to the trends, with correlations of 0.98 for monthly and 0.84 for smoothed values.

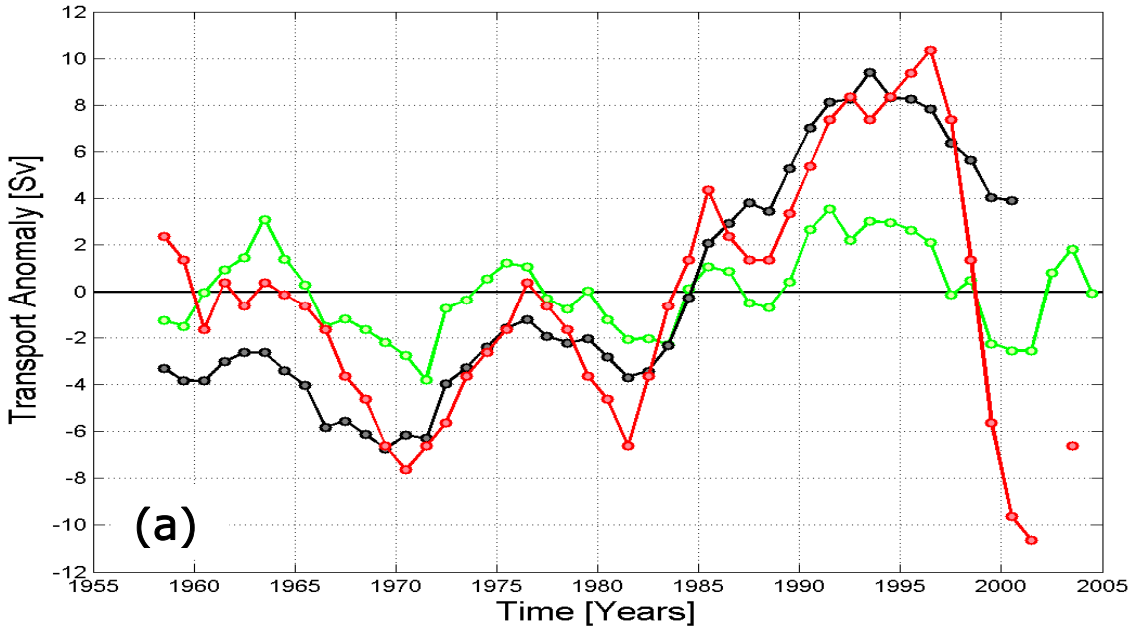

528

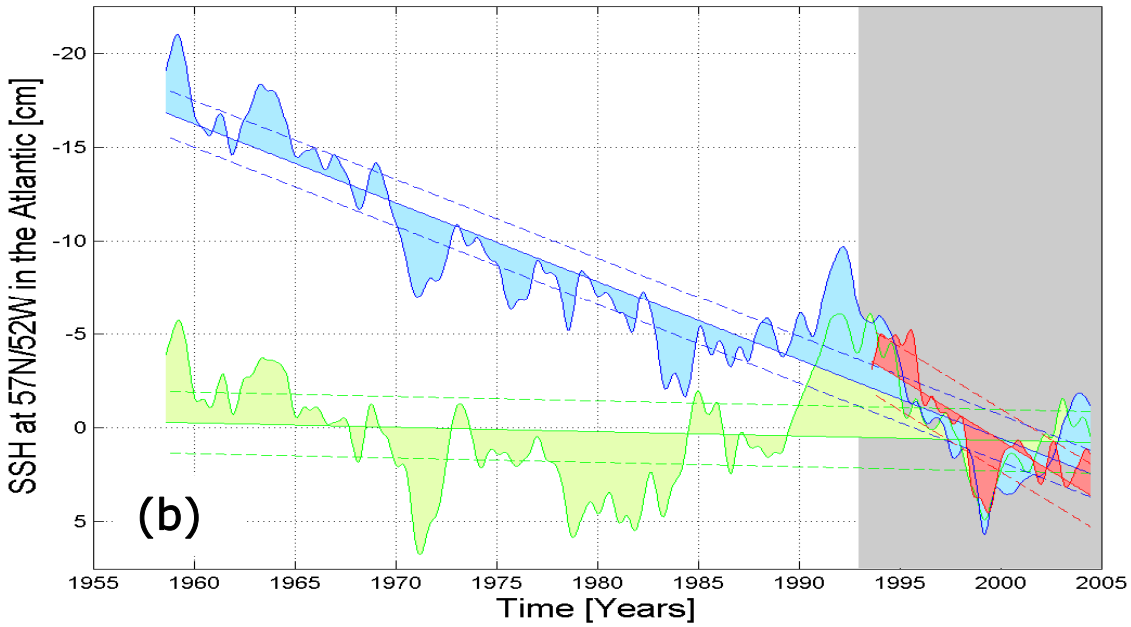

529

530 **Figure 2. Indices of large-scale transport variability. (a)** Index of observed (red) annual
531 mean baroclinic mass transport anomaly between the subpolar and subtropical gyres
532 following *Curry and McCartney* [2001] in comparison to the model simulations CNTRL
533 (green) and CNTRL-GM (black), whereby the amplitude of year-to-year variability amounts
534 to 5.0Sv in the observations, 1.8Sv in CNTRL and 3.8Sv in CNTRL-GM. **(b)** Subpolar gyre
535 index following *Häkkinen and Rhines* [2004] and *Hátún et al.* [2005] as given by the annually

smoothed monthly mean sea level anomaly η_d at 57°N, 52°W in AVISO satellite altimeter data (red), CNTRL (green) and FRESH (blue), with linear trends (solid) and standard deviations of interannual variability (dashed). Note, that the climatological seasonal cycle over the period shaded in grey has been subtracted, resulting in a shift of these "normalized" time series to emphasize the similarity of interannual variability of both model cases and observational data.

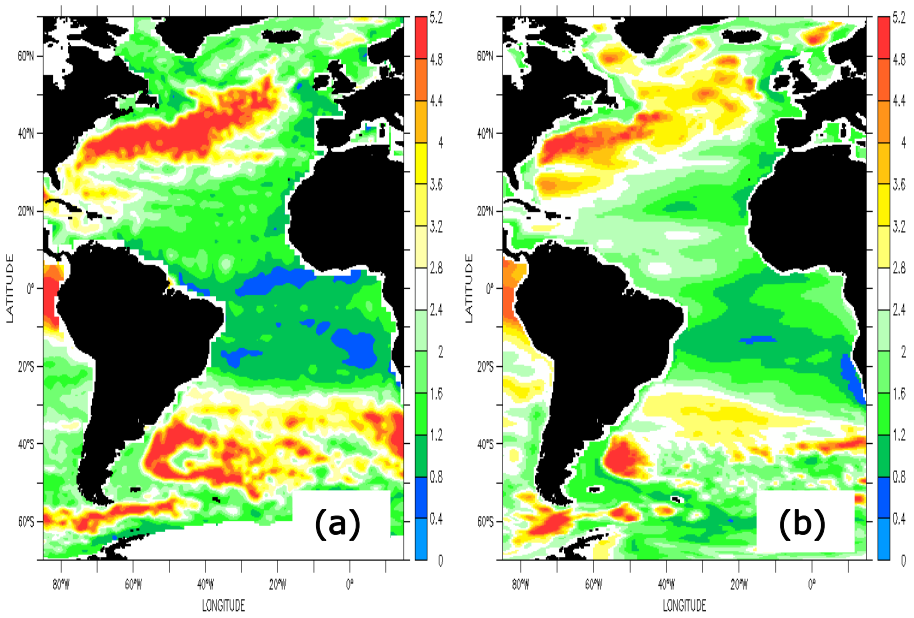

542

543 **Figure 3. Interannual sea level variability: Model vs. altimeter data.** Standard deviation

544 during 1993 to 2004 of annual mean anomalies of dynamic SSH, η_d (in cm): **(a)** AVISO data

545 and **(b)** CNTRL.

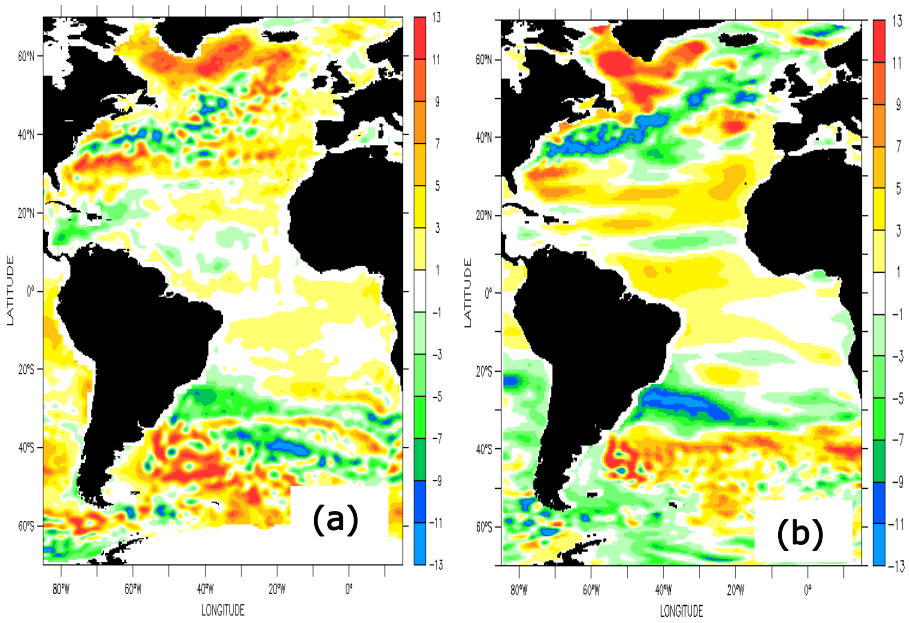

546

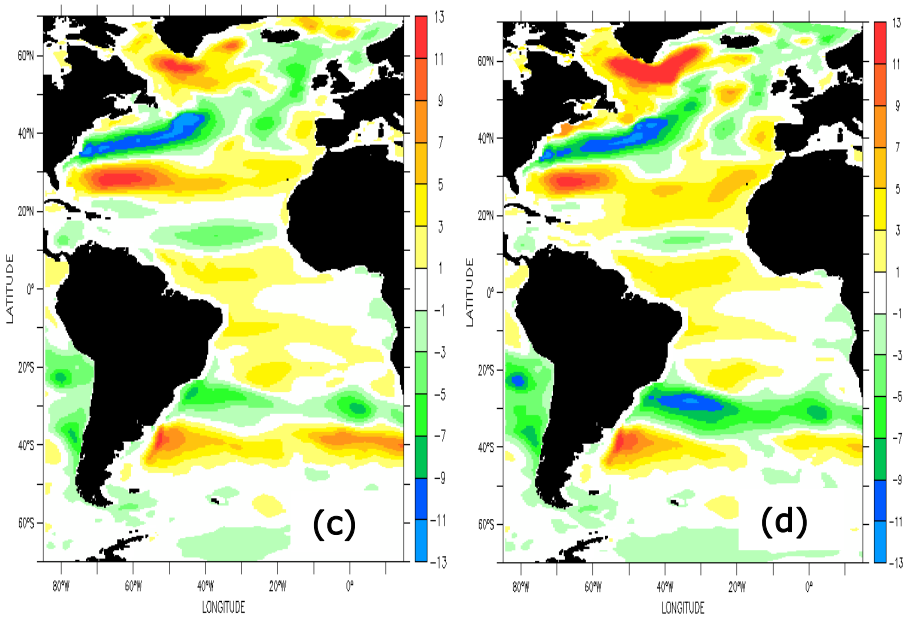

547

548 **Figure 4. Interannual sea level trend: Model vs. altimeter data.** Linear trend (1993-1999)

549 of η_d (in mm/yr) in comparison between **(a)** AVISO data and simulations: **(b)** CNTRL, **(c)**

550 WIND-GM and **(d)** CNTRL-GM.

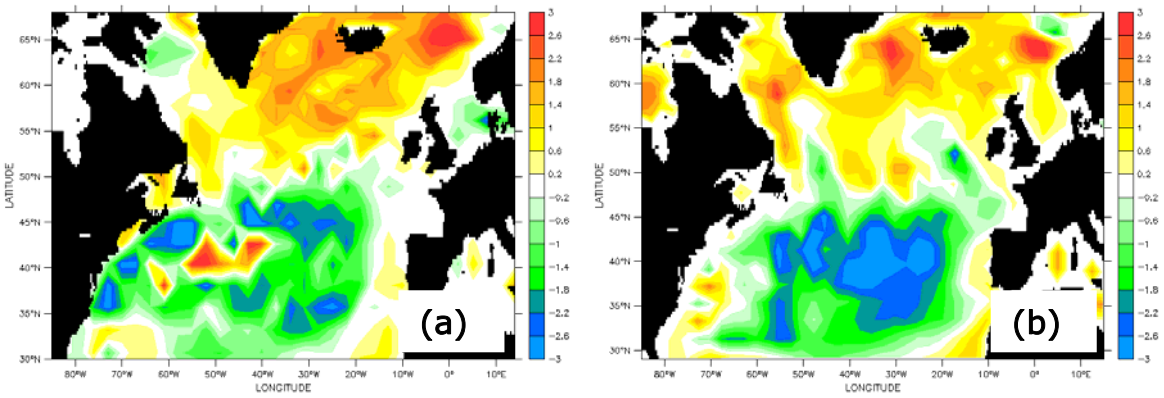

551

552 **Figure 5. Patterns of interannual sea level variability.** First EOF of detrended anomalous

553 annual means of η_d over the observational period (1993-2004) in **(a)** AVISO data and **(b)**

554 CNTRL.

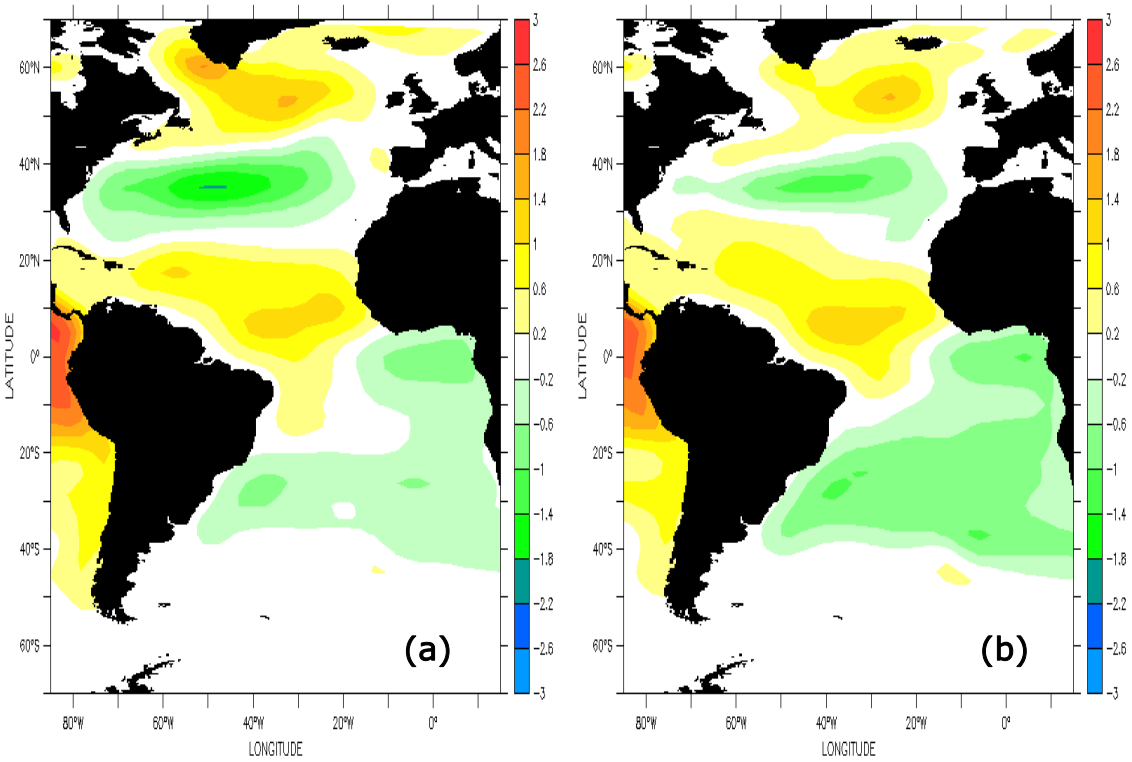

555

556 **Figure 6. Dynamic cause of interannual sea level variability patterns.** First EOF of

557 detrended anomalous annual means of η_d over the hindcasting period (1958-2004) in **(a)**

558 CNTRL-GM and **(b)** WIND-GM.

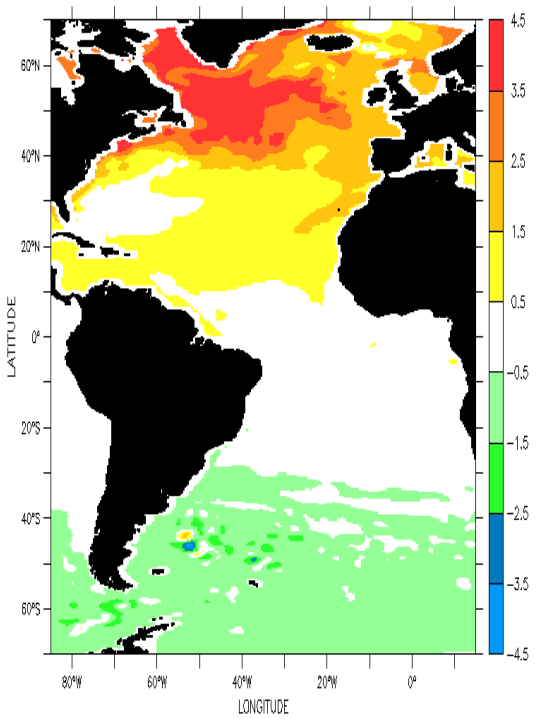

559

560 **Figure 7. SSH changes due to multi-decadal MOC decline.** Linear trend (1958-2004) of

561 η_d (in mm/yr) in FRESH relative to CNTRL.

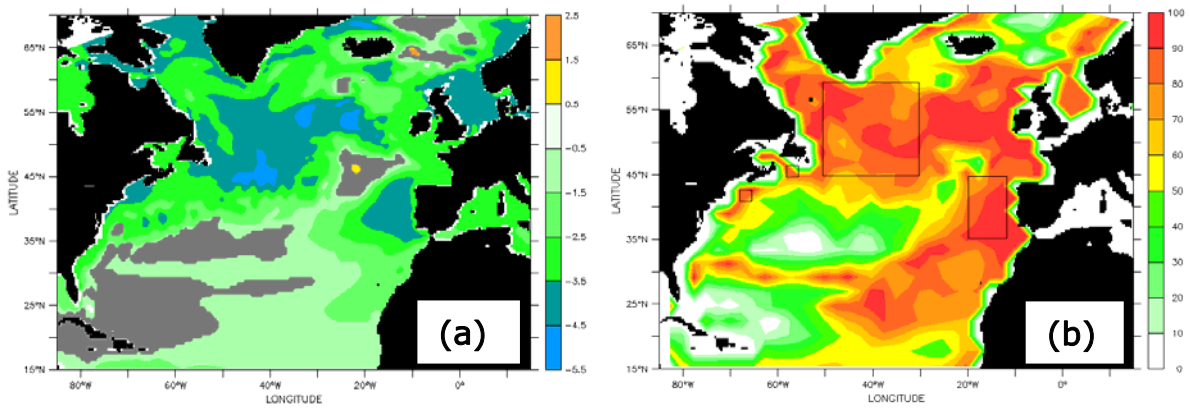

562

563 **Figure 8. Manifestation of multi-decadal MOC decline. (a)** Linear regression (1958-2004)
564 of anomalous annual mean η_d and the MOC-index in FRESH (in cm/Sv); grey areas indicate
565 non-significant values at the *t*-test 95% level **(b)** Percentage of the covariance between local
566 η_d and the MOC-index due to the linear trends in both variables. Boxes indicate regions
567 where we have assessed the detectability of a gradual MOC decline as simulated in FRESH
568 based on continuous records of η_d (Labrador Sea: 57°N/52°W; SPG: average from 45°-60°N
569 and 30°-50°W, "West European" box: average from 35°-45°N and 12°-22°W, and two sites
570 along the North American coast: 41°-43°N/65°-68°W and 45-46°N/56°-58°W).